ChemComm

COMMUNICATION

View Article Online
View Journal

Cite this: DOI: 10.1039/d5cc06492a

Received 15th November 2025,
Accepted 27th January 2026

DOI: 10.1039/d5cc06492a

rsc.li/chemcomm

Fluoride ion chelation *via* pnictogen bonding using a distibora[1.1]ferrocenophane

Arunabha Thakur,*[ab] Brendan L. Murphy,[a] You Jiang,[a] Nattamai Bhuvanesh[a] and François P. Gabbaï *[a]

As part of our interest in anion binding platforms, we now report the synthesis and structure of a neutral distibora[1.1]ferrocenophane, which behaves as a bidentate Lewis acid as demonstrated by its ability to chelate a fluoride anion. This bonding mode, confirmed by single crystal X-ray diffraction, is associated with a fluoride ion affinity of 346 kJ mol^{-1}.

As part of our efforts in the chemistry of bidentate bis-antimony Lewis acids[1] for the chelation of anions *via* convergent pnictogen bonding,[2] we have investigated a family of bifunctional systems featuring catecholatostiboranes as *σ*-hole donors.[3–5] These systems can be accessed with high fidelity through a route involving oxidation of the corresponding distibine with an *ortho*-quinone, typically 3,4,5,6-tetrachloro-1,2-benzoquinone (*o*-chloranil).[6] The success of this approach is illustrated by derivatives such as **A**[3] and **B**[4] (Fig. 1) which were shown to chelate the fluoride anion through the formation of an Sb-F-Sb bridge. To further elaborate this class of compounds, we wondered whether our approach would also be compatible with ferrocene as the backbone. This question was stimulated by prior reports exploring ferrocenylboranes as anion-binding platforms[7] as well as more recent reports of ferrocenylstibines in which the ferrocene fragment survives antimony-centered oxidation by *ortho*-quinones.[8] Against this backdrop and with applications in anion capture and transport as an ultimate objective,[9] we have now set our eyes on ferrocene-based distibines in view of their conversion into the corresponding distiboranes.

Aiming for rigidity, we decided to target a distiba[1.1]ferrocenophane, a class of compounds that has remained unknown even though the diphospha-[10,11] and diarsa-congeners[12] are precedented. In this communication, we report the synthesis and characterization of a distiba[1.1]ferrocenophane and its subsequent oxidation *via* treatment with *o*-chloranil. We further show that the resulting distibora[1.1]ferrocenophane is capable of fluoride anion chelation, which is evident by both NMR spectroscopy and cyclic voltammetry (CV).

To begin, 1,1′-dilithioferrocene·tmeda (tmeda = *N*,*N*,*N*′,*N*′-tetramethylethylenediamine) was reacted with one equiv. of $PhSbCl_2$ which, following column chromatography, afforded the distiba[1.1]ferrocenophane **1** as a yellow-orange solid (Fig. 2a). Compound **1** is a rare example of a ferrocenophane which was isolated directly from the reaction mixture at room temperature without light irradiation of its isolated monomer.[11,13] In the course of fully characterizing this compound, ^{1}H NMR spectroscopy indicated the formation of two distinct species that are differentiated by their cyclopentadienyl (Cp) proton resonances. As has been found for other heteroatom-bridged ferrocenophane species,[11] this suggests the formation of *syn* and *anti*-conformations of distiba[1.1]ferrocenophane **1**. This proposal was confirmed by the crystallization and determination of the solid-state structures of $\mathbf{1}_{syn}$ and $\mathbf{1}_{anti}$ by single-crystal X-ray diffraction (scXRD, Fig. 2b and c) analysis, which indicated that $\mathbf{1}_{anti}$ exists as a centrosymmetrical dimer. Unfortunately, the lack of an adequate amount of isolated pure $\mathbf{1}_{anti}$ precluded its characterization by ^{1}H and ^{13}C NMR spectroscopy. Nevertheless, examination of the solid-state structures demonstrates that the Cp ligands in both $\mathbf{1}_{syn}$ and $\mathbf{1}_{anti}$ are oriented in a nearly eclipsed conformation and that the two ferrocene units of each isomer

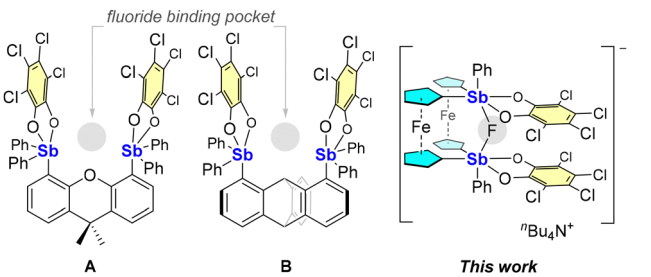

Fig. 1 Selected examples of known catecholatostiborane-based bidentate Lewis acids (**A**) and (**B**) as fluoride anion chelators and structure of the fluoride complex obtained in this work.

[a] *Department of Chemistry, Texas A&M University, College Station, TX 77843, USA. E-mail: francois@tamu.edu*
[b] *Department of Chemistry, Jadavpur University, Kolkata 700032, India*

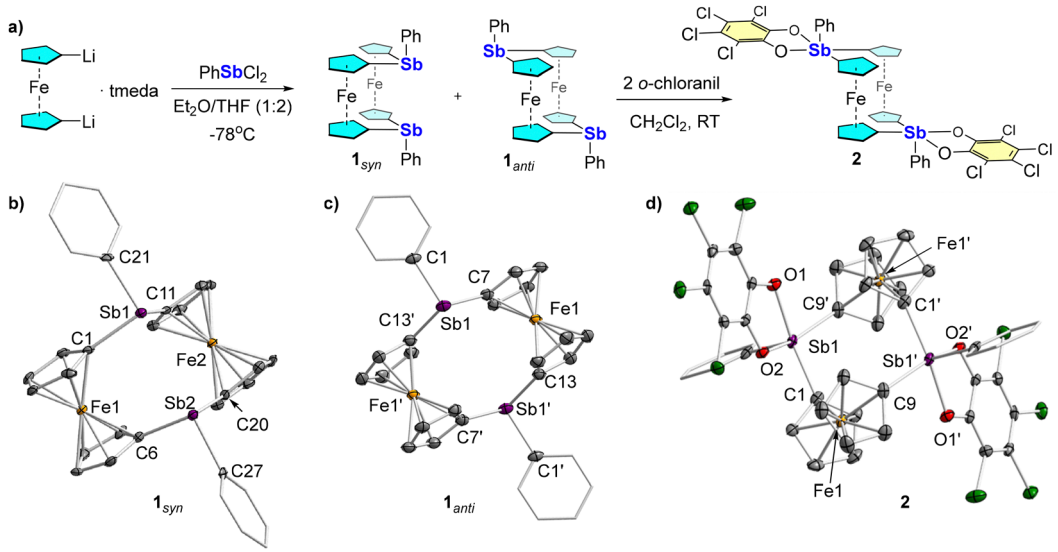

Fig. 2 (a) Synthesis of isomers of **1** and their oxidation to **2**. Solid-state structures of (b) $\mathbf{1}_{syn}$, (c) $\mathbf{1}_{anti}$, and (d) **2**. Thermal ellipsoids are drawn at the 50% probability level. The hydrogen atoms and interstitial solvent molecules are omitted for clarity. Only one of the two independent molecules found in the cell is shown for **2**. Selected atoms are labeled. Selected bond lengths (Å) and angles (°): $\mathbf{1}_{syn}$: Sb1-C1 2.135(4), Sb1-C11 2.133(4), Sb2-C6 2.129(4), Sb2-C20 2.122(5); C1-Sb1-C11 101.8(2), C6-Sb2-C20 99.5(2); $\mathbf{1}_{anti}$: Sb1-C1 2.169(4), Sb1-C7 2.131(4), C1-Sb1-C7 95.05(1); **2** (corresponding metrical parameters of the second independent molecule are given in brackets): Sb1-C1 2.123(3) [2.124 (3)], Sb1-O1 2.075(2) [2.031 (2)], Sb1-O2 2.054(2) [2.104(2)], Sb1-C9 2.103(3) [2.079(3)], C9-Sb1-C1 105.2(1) [106.4(1)], O1-Sb1-O2 77.6(7) [77.8(8)].

stand in registry with one another. The two antimony centers are separated by 3.754(6) Å in the case of $\mathbf{1}_{syn}$; however, the distance between the two stibine centers for $\mathbf{1}_{anti}$ is significantly greater at 5.221(6) Å. In both cases, the antimony atom adopts a trigonal pyramidal geometry with a slightly broader C(Cp)-Sb-C(Cp) angle for $\mathbf{1}_{anti}$ (103.8(1)°) compared to that for $\mathbf{1}_{syn}$ (101.8(2)°). We note that these isomers do not interconvert even upon heating a mixture of $\mathbf{1}_{syn}$ and $\mathbf{1}_{anti}$ to 100 °C in toluene-d_8 (Fig. S5), in contrast to the phosphorus congener.[11]

We next attempted to access the distibora[1.1]ferrocenophane by treating a mixture of isomers of **1** with two equiv. of *o*-chloranil in CH_2Cl_2. This reaction cleanly oxidizes the stibine units to afford compound **2** as a single product in 80% yield (Fig. 2). scXRD analysis reveals that **2** crystallizes with two independent centrosymmetric dimers in the asymmetric unit. Each molecule situates its two Lewis acidic catecholatostiborane centers *anti* to one another (Fig. 2). Given the steric heft of the tetrachlorocatecholate ligand, we contend that the *anti*-conformation lessens the Pauli repulsions bewteen the bulky catecholatostiboranes. In the independent molecule depicted in Fig. 2, the antimony atoms adopt a distorted square-pyramidal geometry ($\tau_5 = 0.06$)[14] with an Sb–Sb separation of 5.113(6) Å. However, we note that both antimony atoms in the second independent molecule adopt a distorted trigonal-bipyramidal geometry ($\tau_5 = 0.68$) with an Sb–Sb separation of 5.368(4) Å. Finally, no evidence for isomerization into the *syn* isomer was obtained, including by ^{1}H NMR spectroscopy in toluene-d_8 at 100 °C (Fig. S12).

With this potential bidentate Lewis acid in hand, we aimed to investigate its fluoride ion affinity (FIA) both computationally and experimentally. Addition of [^{n}Bu$_4$N][PF$_6$] to a $CDCl_3$ solution of **2** did not produce any fluoride adduct, indicating that **2** cannot abstract fluoride from the PF_6^- ion (Fig. S9–S11). However, addition of one equiv. of [^{n}Bu$_4$N][Ph$_3$SiF$_2$] (TBAT) to **2** in CH_2Cl_2 generates the air- and moisture-stable pale-yellow solid [^{n}Bu$_4$N][2-μ_2-F] in 80% yield (Fig. 3a). ^{19}F NMR of this material reveals a single resonance at −32.00 ppm, which is in the range of other fluoride-bridged bis-stiborane species.[3,4] scXRD analysis confirms the chelation of the fluoride anion between the two catecholatostiborane units (Fig. 3b), which now adopt a *syn* orientation with respect to the ferrocenophane scaffold. At this geometry, fluoride anion chelation appears perfectly symmetrical, as indicated by equal Sb1-F1 and Sb2-F1 bonds of 2.147(9) Å, a distance that is on par with the Sb-F separations observed in previously described fluoride complexes of **A** and **B**.[3,4] The resulting Sb1-F1-Sb2 angle of 147.8(4)° is quite oblique,[5] reflecting the close proximity of the two stiborane units (Sb-Sb separation 4.125(1) Å) and the narrow fluoride binding pocket. This is also reflected in the computed FIA of **2** of 346 kJ mol^{-1} which is lower than that of other antimony-based fluoride chelators such a **A** (365 kJ mol^{-1}) and **B** (395 kJ mol^{-1}), which we calculated previously using a marginally different level of theory.[9] To assess the electronic properties of the host at the adduct geometry, we computationally removed the fluoride anion and evaluated the electronic structure of **2** at that geometry. This approach reveals the presence of the antimony-based σ* orbitals that project into the binding pocket of **2** (Fig. 3c). Moreover, the electrostatic potential map (ESP) displays a region of positive potential between the two Lewis acidic centers (Fig. 3d). Both of these findings substantiate that **2** acts as a dual pnictogen bond donor to the fluoride anion.

But unlike **A** and **B**, which have their Lewis acidic centers rigidly predisposed to chelate fluoride, we contend that

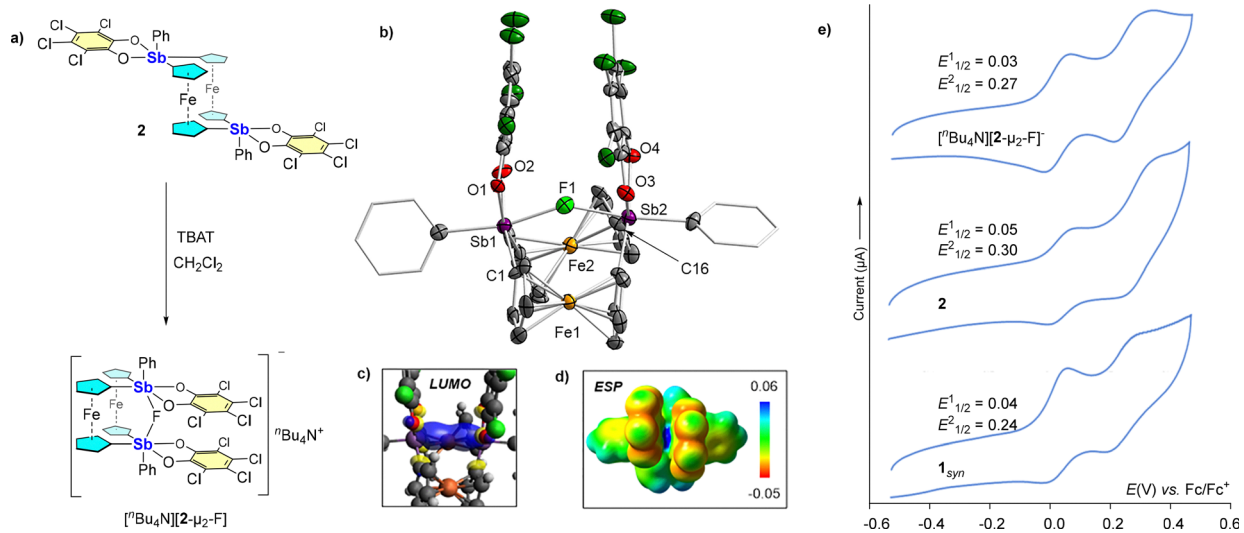

Fig. 3 (a) Synthesis of [^{n}Bu$_4$N][**2**-μ$_2$-F]. (b) Solid-state structure of [^{n}Bu$_4$N][**2**-μ$_2$-F]. Thermal ellipsoids are drawn at the 50% probability level. The hydrogen atoms and interstitial solvent molecules are omitted for clarity. Selected atoms are labeled. Selected bond lengths (Å) and angles (°): Sb1-C1 2.100(1), Sb1-F1 2.147(9), Sb1-O1 2.089(9), Sb1-O2 2.051(1), Sb2-O3 2.078(1), Sb2-O4 2.077(9), Sb2-F1 2.147(9), Sb2-C16 2.177(1); C1-Sb1-F1 87.1(5), C16-Sb2-F1 85.8(5), Sb1-F1-Sb2 147.8(4), O1-Sb1-O2 79.4(4), O3-Sb2-O4 78.4(4). (c) Contour plot of the LUMO of **2** at the fluoride binding geometry (isovalue: 0.05 a.u.). (d) ESP map of [^{n}Bu$_4$N][**2**-μ$_2$-F] (isovalue: 0.03 a.u., gradient scale values given in a.u.). (e) Cyclic voltammogram of compounds **1**$_{syn}$, **2** and [^{n}Bu$_4$N][**2**-μ$_2$-F] (1.0 × 10^{-4} M) in CH_3CN/THF (1 : 1, *v*/*v*) with [^{n}Bu$_4$N][PF_6] as the supporting electrolyte at a scan rate of 0.1 V s^{-1}. Potentials are referenced to Fc/Fc$^+$.

formation of [**2**-μ$_2$-F]$^-$ is templated by the fluoride anion. That is, the fluoride likely first binds to a single antimony center in the *anti* configuration of the free receptor, which subsequently rearranges into the observed *syn* configuration, with the fluoride anion bridging the two antimony centers. We have computed a possible pathway for this process which begins with a highly favorable binding of the fluoride anion to one of the antimony centers of **2** (Fig. 4). Powered by the excess energy of this fluoride-binding step, the resulting intermediate (**Int-1**) proceeds over a 26.2 kcal mol^{-1} barrier, ultimately enabling the required conformational change and subsequent fluoride chelation. This mechanistic proposal hinges on the notion that the excess energy of the first step enables an otherwise prohibitive barrier to be overcome at room temperature. This notion is supported by previous mechanistic investigations where similar arguments have been convincingly advanced.[15]

Finally, the electrochemical behavior of **1**$_{syn}$, **2**, and crystalline [^{n}Bu$_4$N][**2**-μ$_2$-F] was studied by cyclic voltammetry. The voltammogram of **1**$_{syn}$ shows two waves of almost equal height, separated by ∼0.20 V (Fig. 3e, *vide supra*), suggesting two sequential one-electron oxidations of the iron centers. Interestingly, compound **2** shows a perceptible shift towards anodic potential ($\Delta E_{1/2}{}^1$ = 10 mV and $\Delta E_{1/2}{}^2$ = 60 mV), indicating that the ferrocene centers in **2** become more electron-deficient after oxidation of the antimony center by *o*-chloranil. Furthermore, the CV of complex [**2**-μ$_2$-F]$^-$ shows a shift towards cathodic potential ($\Delta E_{1/2}{}^1$ = 20 mV and $\Delta E_{1/2}{}^2$ = 30 mV) with respect to compound **2**, consistent with the chelation of an anionic guest

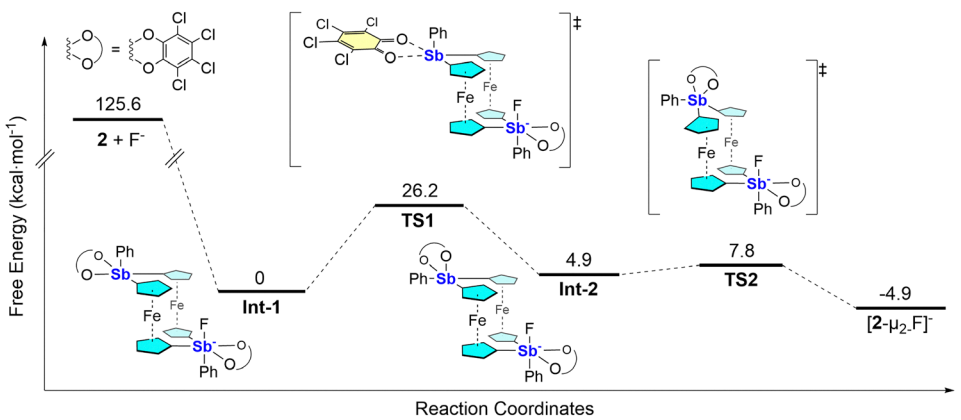

Fig. 4 Computed mechanism leading to the formation of [**2**-μ$_2$-F]$^-$. All energies, the accuracy of which is affected by the level of theory employed, are in kcal mol^{-1}.

that partially screens positive charge development at the iron centers.[16]

This work provides access to a heretofore unknown distiba[1.1]ferrocenophane, which can be accessed by conventional synthetic routes and converted into a distibora[1.1]ferrocenophanes without involvement of the iron centers in the oxidation process. The *anti* structure presented by the latter rearranges upon fluoride binding, to position the catecholatostiborane units in a conformation compatible with the chelation of the fluoride anion *via* convergent pnictogen bonding. The narrow spacing of the Cp ring makes for a rather snug binding pocket, resulting in the puckering of the Sb-F-Sb bridge.

Conflicts of interest

There are no conflicts to declare.

Data availability

The data supporting this article can be found in the supplementary information (SI). Supplementary information: this SI contains synthetic details, characterization data, spectroscopic data, crystallographic details, and computational details. See DOI: https://doi.org/10.1039/d5cc06492a.

CCDC: 2502484–2502487 contain the supplementary crystallographic data for this paper.[17a–d]

Note added in proof

We acknowledge a recent related publication[18] that appeared after submission of this article, and that describes related ferrocene-antimony derivatives, including a stiba[1]ferrocenophane and its polymerization.

Acknowledgements

This work was carried out at Texas A&M University with support from the National Science Foundation (CHE-2505795) and the Welch Foundation (A-1423). AT thanks the India-based Science and Engineering Research Board for awarding him an International Research Experience Fellowship (SIR/2022/000058). All calculations were conducted with the advanced computing resources provided by Texas A&M High Performance Research Computing. Finally, we thank Daniel Singleton for useful discussions.

References

1 (*a*) J. Qiu, B. Song, X. Li and A. F. Cozzolino, *Phys. Chem. Chem. Phys.*, 2018, **20**, 46–50; (*b*) J. L. Beckmann, J. Krieft, Y. V. Vishnevskiy, B. Neumann, H.-G. Stammler and N. W. Mitzel, *Angew. Chem., Int. Ed.*, 2023, e202310439.
2 G. Resnati, D. L. Bryce, G. R. Desiraju, A. Frontera, I. Krossing, A. C. Legon, P. Metrangolo, F. Nicotra, K. Rissanen, S. Scheiner and G. Terraneo, *Pure Appl. Chem.*, 2024, **96**, 135–145.
3 M. Hirai and F. P. Gabbaï, *Angew. Chem., Int. Ed.*, 2015, **54**, 1205–1209.
4 C.-H. Chen and F. P. Gabbaï, *Angew. Chem., Int. Ed.*, 2017, **56**, 1799–1804.
5 D. You, B. Zhou, M. Hirai and F. P. Gabbaï, *Org. Biomol. Chem.*, 2021, **19**, 4949–4957.
6 (*a*) R. R. Holmes, R. O. Day, V. Chandrasekhar and J. M. Holmes, *Inorg. Chem.*, 1987, **26**, 157–163; (*b*) M. Yang, D. Tofan, C.-H. Chen, K. M. Jack and F. P. Gabbaï, *Angew. Chem., Int. Ed.*, 2018, **57**, 13868–13872.
7 (*a*) C. Dusemund, K. R. A. S. Sandanayake and S. Shinkai, *J. Chem. Soc., Chem. Commun.*, 1995, 333–334; (*b*) R. Boshra, K. Venkatasubbaiah, A. Doshi, R. A. Lalancette, L. Kakalis and F. Jäkle, *Inorg. Chem.*, 2007, **46**, 10174–10186; (*c*) A. E. J. Broomsgrove, D. A. Addy, A. Di Paolo, I. R. Morgan, C. Bresner, V. Chislett, I. A. Fallis, A. L. Thompson, D. Vidovic and S. Aldridge, *Inorg. Chem.*, 2010, **49**, 157–173; (*d*) M. J. Kelly, A. E. J. Broomsgrove, I. R. Morgan, I. Siewert, P. Fitzpatrick, J. Smart, D. Vidovic and S. Aldridge, *Organometallics*, 2013, **32**, 2674–2684; (*e*) D. Cao, H. Zhao and F. P. Gabbaï, *New J. Chem.*, 2011, **35**, 2299–2305.
8 (*a*) J. Schulz, J. Antala, D. Rezazgui, I. Císařová and P. Štěpnička, *Inorg. Chem.*, 2023, **62**, 14028–14043; (*b*) B. Zhou, S. Bedajna and F. P. Gabbaï, *Chem. Commun.*, 2024, **60**, 192–195; (*c*) J. Antala, J. Schulz, I. Císařová and P. Štěpnička, *New J. Chem.*, 2024, **48**, 5107–5119; (*d*) D. Rezazgui, J. Schulz and P. Štěpnička, *Inorg. Chem.*, 2025, **64**, 11075–11092.
9 B. L. Murphy and F. P. Gabbaï, *J. Am. Chem. Soc.*, 2023, **145**, 19458–19477.
10 H. Brunner, J. Klankermayer and M. Zabel, *J. Organomet. Chem.*, 2000, **601**, 211–219.
11 T. Mizuta, Y. Imamura, K. Miyoshi, H. Yorimitsu and K. Oshima, *Organometallics*, 2005, **24**, 990–996.
12 C. Spang, F. T. Edelmann, M. Noltemeyer and H. W. Roesky, *Chem. Ber.*, 1989, **122**, 1247–1254.
13 D. E. Herbert, J. B. Gilroy, W. Y. Chan, L. Chabanne, A. Staubitz, A. J. Lough and I. Manners, *J. Am. Chem. Soc.*, 2009, **131**, 14958–14968.
14 A. W. Addison, T. N. Rao, J. Reedijk, J. van Rijn and G. C. Verschoor, *J. Chem. Soc., Dalton Trans.*, 1984, 1349–1356.
15 (*a*) Y. Oyola and D. A. Singleton, *J. Am. Chem. Soc.*, 2009, **131**, 3130–3131; (*b*) L. M. M. Quijano and D. A. Singleton, *J. Am. Chem. Soc.*, 2011, **133**, 13824–13827.
16 (*a*) A. J. Taylor, R. Hein, S. C. Patrick, J. J. Davis and P. D. Beer, *Angew. Chem., Int. Ed.*, 2024, **63**, e202315959; (*b*) R. Hein, A. Docker, J. J. Davis and P. D. Beer, *J. Am. Chem. Soc.*, 2022, **144**, 8827–8836.
17 (*a*) CCDC 2502484: Experimental Crystal Structure Determination, 2026, DOI: 10.5517/ccdc.csd.cc2q0193; (*b*) CCDC 2502485: Experimental Crystal Structure Determination, 2026, DOI: 10.5517/ccdc.csd.cc2q01b4; (*c*) CCDC 2502486: Experimental Crystal Structure Determination, 2026, DOI: 10.5517/ccdc.csd.cc2q01c5; (*d*) CCDC 2502487: Experimental Crystal Structure Determination, 2026, DOI: 10.5517/ccdc.csd.cc2q01d6.
18 H. K. S. Young, H. N. L. Leslie, B. O. Patrick, E. A. LaPierre and I. Manners, *Inorg. Chem.*, 2026, **65**, 2833–2840.

